

# Synthesis and Characterization of some Rare Earth Metals doped Bismuth Copper Titanate Ceramics



Thesis submitted in partial fulfilment  
for the Award of Degree  
**Doctor of Philosophy**

by

**Dinesh Prajapati**

DEPARTMENT OF CHEMISTRY  
INDIAN INSTITUTE OF TECHNOLOGY  
(BANARAS HINDU UNIVERSITY)  
VARANASI-221005

Roll No.: 19051002

2024

## **DECLARATION BY THE CANDIDATE**

I, Dinesh Prajapati, certify that the work embodied in this thesis is my own bonafide work and carried out by me under the supervision of Prof. K. D. Mandal from 2019 to 2024, at the Department of Chemistry, Indian Institute of Technology (Banaras Hindu University), Varanasi. The matter embodied in this thesis has not been submitted for the award of any other degree/diploma. I declare that I have faithfully acknowledged and credited the research professionals whose works have been cited in my thesis. I further declare that I have not wilfully copied any other's work, paragraphs, text, data, results, etc., reported in journals, books, magazines, reports, dissertations, theses, etc., or available on websites, and that they have not been incorporated in my thesis or referenced as my own work.

Date: 22/5/2024

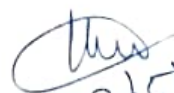
Place: Varanasi

  
Signature of the Student

(Mr. Dinesh Prajapati)

## **CERTIFICATE BY THE SUPERVISOR(S)**


It is certified that the above statement made by the student is correct to the best of my knowledge.

  
22/5/2024

**Prof. K. D. Mandal**  
(Supervisor)

**Department of Chemistry**  
**Indian Institute of Technology**  
**(Banaras Hindu University)**  
**Varanasi**

**Prof. K. D. Mandal**  
Department of Chemistry  
Indian Institute of Technology (BHU),  
Varanasi-221005

  
**Prof. Sundaram Singh**  
(Head)


**Department of Chemistry**  
**Indian Institute of Technology**  
**(Banaras Hindu University)**  
**Varanasi**

विभागाध्यक्ष / HEAD  
रसायन विज्ञान विभाग  
Department of Chemistry  
भारतीय प्रौद्योगिकी संस्थान (का.हि.वि.वि.)  
Indian Institute of Technology (B.H.U.)  
वाराणसी-221005 / Varanasi-221005

## CERTIFICATE

It is certified that the work contained in the thesis titled "Synthesis and Characterization of some Rare Earth Metals doped Bismuth Copper Titanate Ceramics" by "**Dinesh Prajapati**" has been carried out under my supervision and that this work has not been submitted elsewhere for a degree.

It is further certified that the student has fulfilled all the requirements of Comprehensive examination, Candidacy and SOTA for the award of Ph.D. degree.

  
22/5/2024

**Prof. K. D. Mandal**  
(Supervisor)  
Department of Chemistry  
Indian Institute of Technology  
(Banaras Hindu University)  
Varanasi

**Prof. K. D. Mandal**  
Department of Chemistry  
Indian Institute of Technology (BHU),  
Varanasi-221005

## COPYRIGHT TRANSFER CERTIFICATE

**Title of the Thesis:** Synthesis and Characterization of some Rare Earth Metals doped  
Bismuth Copper Titanate Ceramics

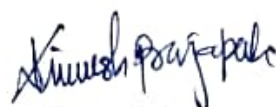
**Name of the Student:** Mr. Dinesh Prajapati

### Copyright Transfer

The undersigned hereby assigns to the Indian Institute of Technology (Banaras Hindu University) Varanasi all rights under copyright that may exist in and for the above thesis submitted for the award of the "Doctor of Philosophy".

Date: 22/5/2024

Place: Varanasi



Signature of the Student

(Mr. Dinesh Prajapati)

**Note:** However, the author may reproduce or authorize others to reproduce material extracted verbatim from the thesis or derivative of the thesis for author's personal use provided that the source and the Institute's copyright notice are indicated.

*It gives me great pleasure to express my gratitude to my supervisor, **Professor K. D. Mandal** of the Indian Institute of Technology's (B.H.U.) Department of Chemistry, for letting me work in his research group and giving me the foundational knowledge for my future. Prof. Mandal is a great advisor and a close friend. He was constantly available for discussions and frequently took the time to address my numerous queries. As a supervisor, he was actively involved in my ongoing education and scientific development, allowing me to conduct studies on various parts of materials science autonomously and with assistance. Furthermore, he provided numerous opportunities for collaboration with other scientists, allowing me to learn more about relevant subjects.*

*My sincere gratitude is also expressed to **Prof. Sundaram Singh**, Head, **Prof. Y. C. Sharma**, Former Head, Department of Chemistry, Indian Institute of Technology, (B.H.U) Varanasi, for their fruitful suggestions and providing research facilities available in the Department.*

*It's my great pleasure to thank my RPEC members **Prof. D. Tiwary**, Department of Chemistry, Indian Institute of Technology, (B.H.U) and **Dr. Shail Upadhyaya**, Department of Physics, Indian Institute of Technology, (B.H.U) for giving valuable suggestions throughout my Ph.D. program.*

*I would like to thank all faculty members of the Department of Chemistry, IIT(BHU) for their support and motivation.*

*I also want to acknowledge the In-charge and members of central instrumentation facility center (CIFC) and office staff of the Chemistry Department for their help and support.*

*I would like to thank my seniors, **Dr. Atendra Kumar** and **Dr. Vinod Kumar**, for their advice during my research work.*

*I also express my sincere thanks to other member of my laboratory companions, **Dr. Alok Kmar Singh**, **Dr. Manish Kumar Verma**, **Dr. Shruti Singh**, **Dr. Santosh Pandey**, **Dr. Vishnu**, **Anup Kumar** and **Biswajit Jena** for their constant help and support.*

*I am very grateful to my best friends, **Mr. Ambuj Kumar Kushwaha**, **Kulveer Singh** and **Kuldeep Kumar Maurya** who helped me a lot during my worst situation, and my seniors from the department, **Dr. Suresh Maurya** and **Dr. Arshala Kamal**, who have also morally supported me throughout this time of difficulty.*

*I would also like to thank my friends batchmates and well-wishers for their motivations and encouragements.*

*Parents are God on earth, and I am truly blessed to have such caring and loving parents in **Mr. Mata Prasad Prajapati** and **Mrs. Moni Devi**. I want to express my gratitude to my family members, particularly my siblings **Mr. Ramesh Prajapati**, **Mr. Rajesh Prajapati**, and **Mr. Abhishek Prajapati** for*

*making my life wonderful with their unwavering affection and spiritual support.*

*I wish to express my special thanks to CSIR New Delhi for providing the financial support to carry out this work.*

*Last but not least, I thank **Almighty God** for providing me strength and courage to do this work.*

*Date: 22/05/2024*

*Place: Varanasi*



*( Dinesh Prajapati )*

	<b>Page No.</b>
<p><b>Fig.1.1</b> Ideal cubic perovskite structure of <math>ABO_3</math> (a) showing corner shared <math>BO_6</math> octahedra and A cation at the interstitial position and (b) showing B cation and <math>BO_6</math> octahedra at the centre of the unit cell.</p>	2
<p><b>Fig.1.2</b> crystal structure of different perovskite unit cells [(a) Cubic, (b) Orthorhombic, (c) Rhombohedral and (d) Tetragonal] in which blue and green color represents A and B cation respectively whereas red color ball represents oxygen atoms.</p>	5
<p><b>Fig.1.3</b> Parallel plate capacitor with the plates separated by distance ‘d’ and area of each plate “A”.</p>	13
<p><b>Fig.1.4</b> Complex impedance plane plot or cole-cole plot and equivalent circuit.</p>	19
<p><b>Fig.1.5</b> The crystal structure of CCTO, highlighting two key features: (a) the Ti-O octahedral network and (b) the <math>CuO_4</math> square planar sublattices. In the illustration, light-blue spheres represent Ti atoms, which are situated at the centers of the octahedra, and red spheres represent O atoms at the corners. The large blue spheres, found at the A sites, indicate the positions of Ca atoms, while the smaller deep-blue spheres at the A' sites signify the positions of Cu atoms.</p>	23
<p><b>Fig.1.6</b> Plot of (a) Dielectric constant and (b) <math>\tan \delta</math> as a function of frequency for Sintered BCTO.</p>	38
<p><b>Fig.2.1.</b> Flow chart for the synthesis of complex perovskite by the semi-wet route.</p>	64

<b>Fig.2.2.</b> Schematic representation of X-ray diffraction from crystal plane	66
<b>Fig.2.3.</b> Powder XRD instrument, Rigaku Miniflex 600 (Japan).	68
<b>Fig.2.4.</b> Schematic representation of the Scanning Electron Microscope.	69
<b>Fig.2.5.</b> Scanning Electron microscopy (SEM, ZEISS model, EVO18 Germany) and EDX Analysis instrument (Oxford instrument; USA).	70
<b>Fig.2.6.</b> Transmission Electron Microscope (TEM, FEI TECANI G <sup>2</sup> 20 TWIN, USA) used to determine particle structure.	72
<b>Fig.2.7.</b> LCR Meter (PSM 1735, Newton 4th Ltd, U.K.) used for dielectric measurement.	75
<b>Fig.3.1.</b> (a) X-ray diffraction (XRD) pattern and (b) Magnified XRD pattern in the enlarged region ( $32^\circ < 2\theta < 36^\circ$ ) of $\text{Bi}_{(2/3)-x}\text{Nd}_x\text{Cu}_3\text{Ti}_4\text{O}_{12}$ BNCTO ( $x = 0.05, 0.10, 0.20$ ) ceramics.	82
<b>Fig.3.2.</b> Rietveld refinement profile of $\text{Bi}_{(2/3)-x}\text{Nd}_x\text{Cu}_3\text{Ti}_4\text{O}_{12}$ ( $x = 0.05, 0.10, 0.20$ ) ceramics.	83
<b>Fig.3.3.</b> (a–c) SEM micrographs and (d-f) EDS spectrum of $\text{Bi}_{(2/3)-x}\text{Nd}_x\text{Cu}_3\text{Ti}_4\text{O}_{12}$ ( $x = 0.05, 0.10, 0.20$ ) ceramics.	85
<b>Fig.3.4.</b> (a-c) 3D AFM image and (d-f) the grain size distribution statistics $\text{Bi}_{(2/3)-x}\text{Nd}_x\text{Cu}_3\text{Ti}_4\text{O}_{12}$ ( $x = 0.05, 0.10, 0.20$ ) ceramics.	86
<b>Fig.3.5.</b> XPS spectra of (a) XPS survey (b) Bi, (c) Nd, (d) Cu, (d) Ti, and (e) O of BNCTO-0.2 ceramic.	88

- Fig.3.6.** (a) Temperature dependence of  $\epsilon'$  and (b)  $\tan \delta$  at 1 kHz of  $\text{Bi}_{(2/3)-x}\text{Nd}_x\text{Cu}_3\text{Ti}_4\text{O}_{12}$  ( $x = 0.05, 0.10, 0.20$ ) ceramics. 89
- Fig.3.7.** (a) Variation of dielectric constant and (b) tangent loss with frequencies for all three concentrations of BNCTO ceramics at 303 K. 91
- Fig.3.8.** (a–c) Variation of  $Z'$  with  $Z''$  at different temperatures and (d) at 303 K of three different concentrations of Nd ( $x = 0.05, 0.10,$  and  $0.20$ ) doped BCTO. 93
- Fig.3.9.** (a-c) Variation of  $Z''$  with frequency at different temperatures and (d) at 303 K of  $\text{Bi}_{(2/3)-x}\text{Nd}_x\text{Cu}_3\text{Ti}_4\text{O}_{12}$  ( $x = 0.05, 0.10, 0.20$ ) ceramics. 94
- Fig.3.10.** (a) Temperature-dependent ac conductivity and (b) Frequency-dependent ac conductivity of BNCTO ceramics. 96
- Fig.4.1.** (a) XRD Pattern and (b) Enlarges view of most intense peak of sintered BSCTO ceramics. 112
- Fig.4.2.** William-Hall Plot of all three Sintered BSCTO ceramics 112
- Fig.4.3.** (a-c) Rietveld analysis of  $\text{Bi}_{(2/3)-x}\text{Sm}_x\text{Cu}_3\text{Ti}_4\text{O}_{12}$  (BSCTO  $x = 0.05, 0.10,$  and  $0.20$ ) ceramics and (d) Crystal representation of BSCTO-0.2 ceramic. 114
- Fig.4.4.** (a-c) SEM micrograph and (d-f) EDS analysis results of BSCTO-0.05, BSCTO-0.1 and BSCTO-0.2 respectively. 117
- Fig.4.5.** (a-c) 3D AFM image and (d-f) Grain size distribution curve of BSCTO-0.05, BSCTO-0.1, and BSCTO-0.2 respectively. 118

- Fig.4.6.** XPS (a) Survey Spectrum, (b) Bi, (c) Sm, (d) Cu, (e) Ti, (f) O, 120  
respectively of BSCTO-0.2 ceramic.
- Fig.4.7.** Variation of (a) dielectric constant and (b) dielectric loss with 121  
temperature at 1 kHz for  $\text{Bi}_{(2/3)-x}\text{Sm}_x\text{Cu}_3\text{Ti}_4\text{O}_{12}$  ( $x = 0.05, 0.10,$   
and 0.20).
- Fig.4.8.** (a) Dielectric constant and (b)  $\tan \delta$  of  $\text{Bi}_{(2/3)-x}\text{Sm}_x\text{Cu}_3\text{Ti}_4\text{O}_{12}$  ( $x$  123  
 $= 0.05, 0.10,$  and 0.20) over a wide range of frequency (20 Hz-  
10 MHz).
- Fig.4.9.** (a-c) Complex impedance plane at different temperatures and 124  
(d) at 303 K for BSCTO-0.05, BSCTO-0.1, and BSCTO-0.2  
ceramics.
- Fig.4.10.** (a) Plots of ac conductivity with temperature ( $1000/T$ ) and (b) 127  
ac conductivity with angular frequency for  $\text{Bi}_{(2/3)-}$   
 $x\text{Sm}_x\text{Cu}_3\text{Ti}_4\text{O}_{12}$  ( $x = 0.05, 0.10,$  and 0.20).
- Fig.5.1.** (a) The XRD patterns and (b) enlargement view of most instance 141  
peaks of  $\text{Bi}_{(2/3)-x}\text{Gd}_x\text{Cu}_3\text{Ti}_4\text{O}_{12}$  ( $x = 0.05, 0.10$  and 0.20)  
ceramics sintered at 1173 K for 8 h.
- Fig.5.2.** Rietveld refinement of XRD profiles of the  $\text{Bi}_{(2/3)-}$  143  
 $x\text{Gd}_x\text{Cu}_3\text{Ti}_4\text{O}_{12}$  ( $x=0.05, 0.10$  and 0.20) ceramic.
- Fig.5.3.** Bright-field TEM images as well as SAED patterns of (a, b) 145  
 $x=0.05,$  (c, d)  $x=0.1$  and (e, f)  $x=0.2$  for  $\text{Bi}_{(2/3)-x}\text{Gd}_x\text{Cu}_3\text{Ti}_4\text{O}_{12}$  ( $x$   
 $= 0.05, 0.10$  and 0.20) ceramics sintered at 1173 K for 8 h

- Fig.5.4.** (a, c) and (b, d), the FE-SEM images of the fractured surfaces and EDX images of  $\text{Bi}_{(2/3)-x}\text{Gd}_x\text{Cu}_3\text{Ti}_4\text{O}_{12}$  ceramics ( $x = 0.10$  and  $0.20$ ) sintered at 1173 K for 8 h. 146
- Fig.5.5.** AFM images of  $\text{Bi}_{(2/3)-x}\text{Gd}_x\text{Cu}_3\text{Ti}_4\text{O}_{12}$  ceramic with a composition of  $x = 0.2$ , (a) two-dimensional image for grain boundary, (b) three-dimensional image for surface roughness, (c) depth histogram graph. 147
- Fig.5.6.** XPS spectra of (a) Bi; (b) Gd; (c) Cu; (d) Ti; (e) O of  $\text{Bi}_{(2/3)-x}\text{Gd}_x\text{Cu}_3\text{Ti}_4\text{O}_{12}$  ( $x = 0.2$ ) ceramic sintered at 1173 K for 8 h. 149
- Fig.5.7.** (a) and (b) the frequency dependence of  $\epsilon'$  and  $\tan \delta$  of  $\text{Bi}_{(2/3)-x}\text{Gd}_x\text{Cu}_3\text{Ti}_4\text{O}_{12}$  ( $x = 0.05, 0.10$  and  $0.20$ ) ceramics sintered at 1173 K for 8 h. 150
- Fig.5.8.** (a) and (b), frequency dependence of imaginary part of impedance ( $Z''$ ) and the complex impedance plot for  $\text{Bi}_{(2/3)-x}\text{Gd}_x\text{Cu}_3\text{Ti}_4\text{O}_{12}$  ( $x = 0.05, 0.10$  and  $0.20$ ) ceramics sintered at 1173 K for 8 h. 152
- Fig.5.9.** (a) and (b) Variation of conductivity with the inverse of temperature at a few selected frequencies and Frequency dependence of AC conductivity at a few selected temperatures of  $\text{Bi}_{(2/3)-x}\text{Gd}_x\text{Cu}_3\text{Ti}_4\text{O}_{12}$  ( $x = 0.05, 0.10$  and  $0.20$ ) ceramics sintered at 1173 K for 8 h. 154

- Fig.6.1.** (a) XRD patterns for  $\text{Bi}_{(2/3-x)}\text{Dy}_x\text{Cu}_3\text{Ti}_4\text{O}_{12}$  ( $x= 0.05, 0.10$  and  $0.20$ ) ceramic ; (b) Inset figure of XRD patterns in enlarged view at the range of  $2\theta$  from  $31^\circ$  to  $33^\circ$ . 167
- Fig.6.2.** Rietveld refined XRD patterns of  $\text{Bi}_{(2/3-x)}\text{Dy}_x\text{Cu}_3\text{Ti}_4\text{O}_{12}$  ( $x= 0.05, 0.10$  and  $0.20$ ) ceramic sintered at  $1173\text{ K}$  for  $8\text{ h}$ . 168
- Fig.6.3.** (a-c) Bright-field TEM image; (e-g) SAED pattern of  $\text{Bi}_{(2/3-x)}\text{Dy}_x\text{Cu}_3\text{Ti}_4\text{O}_{12}$  ( $x= 0.05, 0.10$  and  $0.20$ ) ceramic. 170
- Fig.6.4.** (a-c) SEM of sintered pellet; (e-g) EDX spectrum of  $\text{Bi}_{(2/3-x)}\text{Dy}_x\text{Cu}_3\text{Ti}_4\text{O}_{12}$  ( $x= 0.05, 0.10$  and  $0.20$ ) ceramic. 171
- Fig.6.5.** The XPS spectrum of (a) Bi; (b) Dy; (c) Cu; (d) Ti; (e) O elements present in the BDCTO-0.2 ceramics. 173
- Fig.6.6.** FTIR spectra of Dy doped BCTO system with various concentrations ( $x=0.05, 0.10$  &  $0.20$ ). 174
- Fig.6.7.** Frequency dependence of the (a) permittivity ( $\epsilon'$ ) and (b) dielectric loss ( $\tan \delta$ ) for the Dy doped BCTO ceramics at  $309\text{ K}$  and  $1\text{ kHz}$ . 175
- Fig.6.8.** (a) Angular frequency-dependent  $Z''$  plot and (b) complex impedance plot for BDCTO-0.05, BDCTO-0.1, and BDCTO-0.2 ceramics at  $309\text{ K}$ . 177

---

**Fig.6.9.** (a) Plots of conductivity ( $\ln \sigma_{ac}$ ) with the inverse of temperature at 1 kHz and (b) Variation of  $\ln \sigma_{ac}$  with  $\ln \omega$  at 309 K for  $\text{Bi}_{(2/3-x)}\text{Dy}_x\text{Cu}_3\text{Ti}_4\text{O}_{12}$  ( $x= 0.05, 0.10$  and  $0.20$ ) ceramic.

---

---

*LIST OF SYMBOLS/ ABBREVIATION*

$t$	Tolerance factor
$\mu$	Octahedral factor
$\eta$	Atomic packing fraction
$E$	Electric field
$\epsilon_0$	Permittivity of free space
$P$	Electrical dipole moment
$\chi_e$	Dielectric susceptibility
$E_{loc}$	Local field
$P_{mol}$	Moment
$\alpha$	Polarizability
$\epsilon^*$	Complex Quantity of dielectric constant
$\epsilon'$	Real components of dielectric constant
$\epsilon''$	Imaginary component of dielectric constant
$i$	Imaginary number
$D$	Dissipation factor
$\tan \delta$	Tangent loss
$W$	Energy loss
$\epsilon_r$	Relative dielectric constant
$C$	Capacitance
$F$	Farad
$\sigma$	Conductivity

---

---

*LIST OF SYMBOLS/ ABBREVIATION*

$E_a$	Activation Energy
$f$	Frequency
$P_{\text{electronic}}$	Electronic polarization
$P_{\text{ionic}}$	Ionic polarization
$P_{\text{molecular}}$	Molecular polarization
$P_{\text{interfacial}}$	Interfacial polarization
Hz	Hertz
$\lambda$	Wavelength
$\theta$	Angle theta
$\beta$	Full Width at Half Maximum
$^{\circ}\text{C}$	Degree centigrade
K	Kelvin
$k_B$	Boltzmann constant
$P$	Net polarization
$\omega$	Angular frequency
$\tau$	Relaxation time
$\text{\AA}$	Angstrom
R	Resistance
C	Capacitance
$Z^*$	Complex impedance
$Z'$	Real impedance
$Z''$	Imaginary impedance

*LIST OF SYMBOLS/ ABBREVIATION*

---

Å	Angstrom
R	Resistance
R <sub>g</sub>	Resistance of grain
R <sub>gb</sub>	Resistance of grain boundary
eV	electron Volt

	Page No.
<b>Table.1.1.</b> ABO <sub>3</sub> perovskite compounds and its applications.	10
<b>Table.1.2.</b> Shows polarization mechanism of dielectric materials.	16
<b>Table.2.1.</b> Specification of the chemicals used.	63
<b>Table.3.1.</b> describes conditions of refinements, the refined parameters calculated through the Rietveld refinements such as Chi-square, space group, Bragg's- R factor, RF-factor, Lattice parameters, FWHM parameters, and conventional Rietveld R-factors of BNCTO ceramic with Nd compositions 0.05,0.1 and 0.2, respectively.	84
<b>Table 4.1.</b> The comparison of crystallite size by Debye-Scherrer Method and Williamson-Hall Plot of BSCTO ceramics	113
<b>Table 4.2.</b> Chi-square( $\chi^2$ ), space group, Lattice parameters, Vcell, FWHM parameters, Conventional Rietveld R-factors, Bragg's- R factor, RF-factor and structural parameter of BSCTO ceramic with the concentration of 0.05, 0.10, and 0.20, respectively.	115
<b>Table 5.1.</b> Conditions for refinement, chi-square ( $\chi^2$ ), Phase, Crystallite size, reliability factor ( $R_p$ , $R_{wp}$ , $R_{exp}$ ), Full-width at half maximum (FWHM) parameters, Bragg R-factor (%), RF-factor (%) and Lattice parameters for BGCTO-0.05, BGCTO-0.1 and BGCTO-0.2 ceramics.	144
<b>Table 5.2.</b> Representing comparative table of the obtained dielectric constant and dielectric loss between the current work and the reported work	150

## *LIST OF TABLES*

---

<b>Table 6.1.</b> Bragg R-factor, RF-factor lattice parameters, crystal structures, angles for $\text{Bi}_{(2/3-x)}\text{Dy}_x\text{Cu}_3\text{Ti}_4\text{O}_{12}$ ( $x = 0.05, 0.10$ and $0.20$ ) ceramic.	169
<b>Table 6.2.</b> Atomic percentage of elements for $\text{Bi}_{(2/3-x)}\text{Dy}_x\text{Cu}_3\text{Ti}_4\text{O}_{12}$ ( $x = 0.05, 0.10$ and $0.20$ ) sintered ceramic	172

Materials science and technology have perpetually occupied a central role in the advancement of any progressive society. The evolution of electro-ceramic materials has notably expanded their potential for diverse applications, spanning optical, structural, environmental remediation, and sensor technologies. Among these, electro-ceramics featuring perovskite oxides/structures  $ABO_3$  have emerged as a significant class of compounds, due to their numerous incredibly interesting chemical, mechanical, thermal, physical, magnetic, and optical properties. A variety of partial substitutions on the A- or B-sites, as well as simultaneous substitutions, can alter the characteristics of the perovskite. Substitutions can be expressed as  $A_{1-x}A'_xBO_3$ ,  $AB_{1-x}B'_xO_3$ , and  $A_{1-x}A'_xB_{1-x}B'_xO_3$ , respectively. These substitutions can be heterovalent, isovalent, or valence compensated in perovskite oxide. It is well understood that the substituent's valency, radius, and coordination number are significant parameters in determining the location where it occupies in the perovskite oxide with a limited composition range to produce a solid solution. Ceramic materials having a high dielectric constant and good thermal stability have received a lot of interest, primarily for their use in electronic devices such as memory devices, gas sensors, humidity sensors, and capacitors.

Calcium copper titanate (CCTO) has the chemical formula  $CaCu_3Ti_4O_{12}$ , a novel electroceramic material with a high dielectric permittivity ( $\epsilon'$ ) of roughly 100,000 for single crystals and 10,000 for bulk materials at ambient temperature. CCTO exhibits minimal dielectric loss ( $\tan \delta \sim 0.15$ ) across a large frequency range (up to  $10^6$  Hz) and maintains phase transition stability at temperatures ranging from 100 to 400 K. In 2000, Subramanian et al. discovered that CCTO belongs to the family of  $ACu_3Ti_4O_{12}$  ( $A = Ca, Sr, Ba, Bi_{2/3}, Y_{2/3}, La_{2/3}$ )-type oxide of the pseudo-cubic perovskite-related structure (space group:  $Im\bar{3}$ ) with a lattice parameter of 7.391 Å. CCTO's high  $\epsilon$  value, which remains constant at temperatures ranging

from 100 to 400 K, makes it suitable for an array of applications. The advancement of technology necessitates a material with a high  $\epsilon$  value to shrink the size of electronic components, while the efficient performance of these components requires a significantly low  $\tan \delta$ . Despite CCTO possessing a very large dielectric constant, its main drawback, especially for undoped CCTO and its related materials, is a slightly high dielectric loss at room temperature. Numerous research studies have been reported on CCTO aimed at reducing dielectric loss by modifying its intrinsic and extrinsic behavior through various methods such as different cationic substitutions or doping at various sites of CCTO, synthetic techniques, and processing parameters to create ideal capacitor materials.

$\text{Bi}_{2/3}\text{Cu}_3\text{Ti}_4\text{O}_{12}$  (BCTO), a member of the  $\text{CaCu}_3\text{Ti}_4\text{O}_{12}$  (CCTO) family, exhibits a similar structure. It has been synthesized using various methods and has shown a very high dielectric constant. However, a high tangent loss was also observed at room temperature, rendering it unsuitable for practical applications. To address this issue, we have chosen the ion doping or substitution method to reduce the tangent loss of the ceramic material. We have reported here the results of our investigation on a class of compounds having perovskite-related structure. These have dielectric properties very different from those of ferroelectrics or relaxors. Their high dielectric constant shows only a small dependence on temperature.

In the current study, various rare earth elements such as neodymium (Nd), samarium (Sm), gadolinium (Gd), and dysprosium (Dy) doped Bismuth Copper Titanate ( $\text{Bi}_{2/3}\text{Cu}_3\text{Ti}_4\text{O}_{12}$ ) (BCTO) ceramic were produced using a well-known semi-wet approach that avoided the need of expensive titanium isopropoxide  $\text{Ti}(\text{OR})_4$ . In this process, metal nitrates and acetates of Bi, Cu, Nd, Sm, Gd, and Dy were combined with  $\text{TiO}_2$  powder. These materials were synthesized using this approach at lower temperatures and in a shorter time. All synthesized materials were

characterized using multiple physicochemical approaches to describe microstructure, crystal structure, particle size and shape, elemental analysis, surface roughness, dielectrics, and electrical characteristics in detail.

The present work aims to synthesize Nd, Sm, Gd, and Dy-doped BCTO ceramics and describe the crystal structure, microstructure, elemental analysis, surface roughness, dielectric and electrical behavior of the following systems:

- $\text{Bi}_{(2/3-x)}\text{Nd}_x\text{Cu}_3\text{Ti}_4\text{O}_{12}$  (BNCTO,  $x= 0.05, 0.10, 0.20$ )
- $\text{Bi}_{(2/3-x)}\text{Sm}_x\text{Cu}_3\text{Ti}_4\text{O}_{12}$  ( BSCTO,  $x= 0.05, 0.10, \text{ and } 0.20$ )
- $\text{Bi}_{(2/3-x)}\text{Gd}_x\text{Cu}_3\text{Ti}_4\text{O}_{12}$  (BGCTO,  $x= 0.05, 0.10 \text{ and } 0.20$ )
- $\text{Bi}_{(2/3-x)}\text{Dy}_x\text{Cu}_3\text{Ti}_4\text{O}_{12}$  (BDCTO,  $x= 0.05, 0.10 \text{ and } 0.20$ )

To the best of our knowledge, there has been no report in the literature on these substituted materials synthesized using this unique approach. A brief description of the research work presented in the thesis divided into seven chapters has been given as follows:

**Chapter 1** This chapter contains a general introduction to the subject describing briefly the technical investigation reported in the field of perovskite oxides complex perovskite oxides and ceramic materials. This chapter includes the effect of various substitutions such as heterovalent, isovalent, and valence compensated substitutions on the dielectric and electrical properties of the materials, and the purpose of the thesis is also mentioned in this chapter.

**Chapter 2** described the experimental procedure used for the preparation and characterization of the complex perovskite oxides. The semi-wet route was used for the preparation of materials with the help of a flow chart. Powder X-ray diffraction (XRD) and retravel refinement have been used to determine the crystallite size and phase formation of

materials. Transmission electron microscope (TEM) coupled with selected area electron diffraction pattern (SAED) have been used for the determination of particle size and crystalline behavior of the material respectively. Scanning electron microscope (SEM) and energy dispersive X-ray spectroscopy (EDX) analysis have been used to examine the surface microstructure and elemental composition of the samples. Surface roughness and average grain size of the materials can be measured by using atomic force microscopy (AFM) techniques. X-ray photoemission spectroscopy (XPS) was used to analyze the valence state of elements present in the ceramics. Using a high-performance frequency LCR meter (E4980A/AL, Keysight, Malaysia) with a frequency range of 20 Hz to 2 MHz, dielectric and electrical measurements were carried out at various temperatures (303 K-503 K). Dielectric properties and electrical properties which are characteristic of all ceramics were also measured with the help of LCR meter with the variation of temperature and frequency (100 Hz-5 MHz).

**Chapter 3** The detailed synthesis, characterization, and application of  $\text{Bi}_{(2/3)-x}\text{Nd}_x\text{Cu}_3\text{Ti}_4\text{O}_{12}$  (BNCTO) ceramic with composition ( $x= 0.05, 0.1, \text{ and } 0.2$ ) prepared by semi-wet route and sintered at 1173 K for 8 h were described in this chapter. X-ray diffraction (XRD) pattern emphasized the single-phase formation up to  $x = 0.05\text{-}0.1$  without any signature of secondary phase, however small amount of secondary phase of rutile phase of  $\text{TiO}_2$  was also deducted by XRD with the composition  $x = 0.2$ . This impurity phase was also confirmed with the help of Rietveld analysis of XRD data. The average grain size was determined from scanning electron microscope (SEM) of BNCTO ceramics decreases with a rise in composition and is found to be  $0.83 \mu\text{m}$ ,  $0.65 \mu\text{m}$ , and  $0.641 \mu\text{m}$ , respectively. The stoichiometry, purity, and the presence of elements (Bi, Cu, Nd, Ti, and O) of synthesized samples were confirmed by EDX studies. AFM analysis shows a reduction in surface root mean square roughness

(Rrms) as the proportion of  $\text{Nd}^{3+}$  ions increases, with corresponding values of 255 nm, 158 nm, and 125 nm, respectively, and average grain size also decreases which validates the SEM result. XPS spectroscopy confirmed the oxidation state of the elements present in the ceramic. Surprisingly, Nd doping can result in an exceptionally low dielectric loss ( $\tan \delta$ ), with a minimum value of 0.05 at 1 kHz and 303 K for BNCTO-0.2. These findings show that Nd doping is more favorable to dielectric characteristics, introducing increased grain boundary resistance, activation energy, and lower conductivity. The detailed temperature and frequency dependence of dielectric properties and conductivity of BNCTO ceramic were disclosed in this chapter

**Chapter 4** This chapter describes the dielectric and electrical properties of  $\text{Bi}_{(2/3)-x}\text{Sm}_x\text{Cu}_3\text{Ti}_4\text{O}_{12}$  (BSCTO) with  $x=0.05, 0.10$  and  $0.20$ . Compositions were synthesized by a low-temperature semi wet route and sintered at 1173 K for 8 h. X-ray powder diffraction analysis unequivocally confirmed the formation of a monophasic BCTO cubic phase without any discernible secondary phases and the crystallite size of the BSCTO ceramic, obtained by X-ray diffraction using Debye Scherrer formula, range from 62 to 81 nm. Rietveld analysis reveals that ceramics have a body centered cubic structure with space group  $\text{Im-3}$ . Scanning electron microscopy (SEM), energy dispersive X-ray spectroscopy (EDS), atomic force microscope (AFM), and X-photoelectron spectroscopy (XPS) were used to study the surface morphology, elemental compositions, surface roughness, and electronic state, respectively. At room temperature and 1 kHz, the composition ( $x = 0.2$ ) has a dielectric constant of around 152 and a dielectric loss of 0.04, respectively. Impedance characteristics revealed a substantial increase in grain boundary resistance, leading to improved dielectric loss. The AC conductivity

of BSCTO ceramics exhibited a frequency-dependent increase satisfying Johncher's power law.

**Chapter 5** The effect of Gd doping in  $\text{Bi}_{2/3}\text{Cu}_3\text{Ti}_4\text{O}_{12}$  ceramic was described in this chapter. Samples of  $\text{Bi}_{(2/3-x)}\text{Gd}_x\text{Cu}_3\text{Ti}_4\text{O}_{12}$  (BGCTO,  $x=0.05, 0.10$  and  $0.20$ ) were synthesized by semi-wet route and sintered at 1173 K for 8 h. Single phase formation with cubic phase of the sintered material was confirmed by X-ray diffraction (XRD) analysis. Rietveld refinement revealed that the material has a BCC structure with space group Im-3. The particle size and crystalline nature of BGCTO ceramic were confirmed by the TEM analysis and SEAD pattern. Further, particle size was determined with the help of Image J software and found to be  $90.85\pm 5$  nm,  $75.35\pm 5$  nm, and  $72.43\pm 5$  nm, respectively for BGCTO ceramic with composition ( $x=0.05, 0.10$ , and  $0.20$ ). The Scanning electron microscope (SEM) images show that the surface morphology consists of plates and spherical grains and EDX analysis confirmed the presence of Bi, Gd, Cu, Ti, and O with their atomic and weight percentage. The oxidation state of the elements which is present in the BGCTO ceramic was validated by XPS analysis. A detailed discussion of temperature and frequency dependent dielectric constant and dielectric loss, electrical, and impedance studies were widely discussed in this chapter.

**Chapter 6** Synthesis of Dysprosium doping at the site of bismuth is discussed in this chapter.  $\text{Bi}_{(2/3-x)}\text{Dy}_x\text{Cu}_3\text{Ti}_4\text{O}_{12}$  (BDCTO,  $x=0.05, 0.10$  and  $0.20$ ) BDCTO ceramic with compositions  $x = 0.05, 0.10$ , and  $0.20$  as designated BDCTO-0.05, BDCTO-0.1, and BDCTO-0.2 respectively, were synthesized through semi wet route and at a sintering temperature of 1173 K for 8 h. The X-ray diffraction pattern and Rietveld analysis reveal the occurrence of all the peaks of parent BCTO ceramic which confirm the formation of a single phase on doping of Dy up to composition 0.2 with the fine crystal structure and have space group Im-3. The

particle size of the BDCTO ceramics obtained from the transmission electron microscopy images was found in the ranges of 80–101 nm. The average grain sizes obtained by SEM of the BDCTO-0.05, BDCTO-0.1, and BDCTO-0.2 ceramics were found to be 123.44 nm, 125.36 nm, and 132.11 nm, respectively. Elemental analysis was performed by EDX that confirmed the presence of all elements in the ceramic with their atomic percentage. The presence of Bi-O, Ti-O, and Ti-O-Ti stretching bands in the ceramic was confirmed by a Fourier transform infrared (FTIR) study. The oxidation state of various ions was studied using X-ray photoelectron spectroscopy. Temperature and frequency dependent dielectric constant, dielectric loss, and conductivity were also extensively studied. Impedance analysis reveals the presence of electrically heterogeneous behavior of the synthesized ceramics.

**Chapter 7** describes the summary of the present research work and its future scope.